




# A Novel Linear Resolver Proposal and its Performance Analysis Under Healthy and Asymmetry Air-gap Fault

Peyman Naderi , Arman Ramezannezhad , Lieven Vandeveld 

**Abstract**—A novel linear resolver is proposed in this paper. The excitation and signals windings are placed on the mover, and the stator structure is designed by a certain number of teeth/slots per the mover length. Therefore, the proposed structure is more simple compared to other resolver types and causes a low price structure. A flexible Magnetic Equivalent Circuit (MEC) is used for analysis thanks to its capability, introducing various structures. The resolver performance under healthy and faulty cases is evaluated, where the position error under asymmetry air-gap fault is obtained. Performed analysis shows that the proposed resolver has less than 100  $\mu\text{m}$  position error. Hence it can be a proper alternative as an accurate position sensor. The simple structure and high-accurate position estimation are the advantages of the proposed resolver compared to other types. Finally, the effectiveness of the proposed resolver is validated by experimental results.

**Index Terms**—Asymmetry air-gap, Absolute Position Error (APE), linear resolver, Magnetic Equivalent Circuit (MEC), Maximum Position Error (MPE).

## I. INTRODUCTION

**T**HE Linear Resolver (L-Resolver) is a well-known position sensor used in industry for special applications such as robotic and vehicular technology. Although the linear encoder is another well-known position sensor, it is not usable in high-temperature and polluted environments [1]. Linear Variable Differential Transformers (LVDTs) are frictionless linear position sensors with reasonable accuracy, but their measurement ranges are limited to  $\pm 25$  cm [2]. The position sensing in the linear or rotational resolvers is based on the induced voltage in two sine and cosine windings that are applied to the Resolver to Digital (R/D) converter [3]. The excitation flux is produced by a third winding that is excited by a high-frequency voltage [3], [4]. Although the resolvers are known as accurate position sensors, a position error can

be produced due to non-ideal output signals. In [3], DC offset error, scale error, and phase error are classified and a compensation method is proposed for accuracy improvement. In most resolvers, the winding arrangement is an important factor for the resolver performance and its influence on accuracies are analyzed in [5], [6]. Moreover, the rotor shape is another important property that is studied in [7], [8]. These factors have the same influences on both rotary and linear resolvers. However, the end-effect and the windings' non-equal magnetic circuit cause some differences between the linear resolver's performance and rotary types [6]. Although there are some presented researches in the resolvers analysis, few works are presented for the linear resolvers compared to the rotary type. The linear resolvers are categorized into two types. The first type has a Variable Reluctance (VR) structure [6], [9], where the windings are located on the mover, and the stator is designed based on the sinusoidal air-gap permeances. The second type is designed based on the slots/teeth stator structure, where the windings are placed on both mover and stator [10]–[13]. However, an additional structure is proposed in [14], where slotted and sinusoidal area solid cores are used. Since the end-effect has considerable influence on the linear resolvers, its modeling is an important issue that should be considered. This effect is considered in [6], [13], where a Magnetic Equivalent Circuit (MEC) is used in [6], and two additional air zones are defined in both the entrance and front parts of the mover. In [13], [15], the subdomain method is used for modeling, which considers the end-effect, but the core nonlinearity effect is omitted. In both investigations, a slotted core linear resolver is employed, and the capabilities of the subdomain method for modeling purposes are proved. In both investigations, the slotted core is considered for a linear resolver, and the subdomain method capability is proved for the modeling purpose. The two Degree of Freedom (2DoF) resolver is another new type of resolver that can measure the rotary and linear position [16], [17], where a MEC and the Finite Element Method (FEM) are used for analysis, respectively. FEM is used many times for this aim, but has two significant drawbacks: long processing simulation time and intensive processing. The challenges of FEM for the resolver analysis are presented in [18]. By noticing the performed researches, there are four conventional methods for the resolvers analysis. Magnetic Equivalent Circuit (MEC) [5], [6], [16], [19], [20], Winding Function Approach (WFA) [21], [22], subdomain method [13], [15], and Finite Element

Manuscript received Month xx, 2xxx; revised Month xx, xxxx; accepted Month x, xxxx. This work was supported in part by the xxx Department of xxx under Grant (sponsor and financial support acknowledgment goes here).

Peyman Naderi (corresponding author) is with the Electrical Engineering Department, Shahid Rajaei Teacher Training University, Tehran, 1631854441, Iran, (e-mail: p.naderi@sru.ac.ir).

Arman Ramezannezhad is Ph.D. student in the Electrical Engineering Department, Shahid Rajaei Teacher Training University, Tehran, 1678815811, Iran. (e-mail: armanramzannezhad@sru.ac.ir).

Lieven Vandeveld is Professor in the Department of Electromechanical, Systems and Metal Engineering of Ghent University, Ghent, Belgium. (e-mail: lieven.vandeveld@ugent.be).

Method (FEM) [18] are used by researchers for designing, optimizing, or analyzing the resolver models. Although FEM is a powerful method, the iterative simulations make the process less suitable compared to a flexible MEC method. A flexible MEC method for a linear structure is proposed in [6], [23] for a Variable Reluctance Linear Resolver (VR-L-Resolver) and Linear Induction Machine (LIM), respectively. The flexible MEC method is applied in the mentioned works while the end-effect and the core nonlinearity are considered for a dynamic model. This method is considered now for the analysis of a new type linear resolver. Since several structures of the proposed resolver are analyzed, the presented flexible MEC method in [23] is used for analysis. Moreover, details of the computational parts can be found in [6], [23]. By noticing to the performed researches, the paper novelties can be summarized as follows:

- ⊗ A new type of a L-Resolver is presented in this work (see Figs. 1 and 2b).
- ⊗ Performance analysis of the presented L-Resolver under healthy and faulty cases with asymmetry air-gap fault (see Fig. 2a).
- ⊗ Position error evaluation under various structures (see Fig. 2b) and analysis of the asymmetry gap fault.

## II. PROPOSED L-RESOLVER

The proposed L-Resolver is illustrated in Figs. 1 and 2b, where the faulty case under asymmetric air-gap fault is illustrated in Fig. 2a. As shown in Fig. 1, six coils are required to obtain the signals ( $A1$ ,  $A2$  and  $B1 - B4$ ) and excitation ( $f1 - f6$ ) units, where the excitation winding has a toroidal configuration. It is a key note that two and four windings are considered for the  $A$  and  $B$  windings, where different turns are used for each signal winding. The winding diagrams are illustrated in Table I for a single stage resolver, where  $N_s$  and  $N_f$  denote the number of turns for the signals and excitation windings, respectively. A multistage resolver is composed of some single-stage resolvers which are connected consecutively (see Fig. 2b). It will be shown that the multistage resolver has higher accuracy and lower sensitivity to the air-gap asymmetry thanks to end-effect mitigation and also mitigation of non-equal magnetic circuit of the signal windings. Although overlapping in the windings diagrams is the only drawback of the proposed resolver, having a low-cost and straightforward structure is the most valuable part of the design. Moreover, it will be shown that the proposed resolver

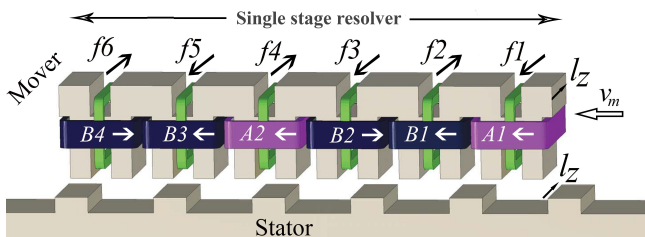


Fig. 1. Proposed linear resolver in the single stage structure as a sample case

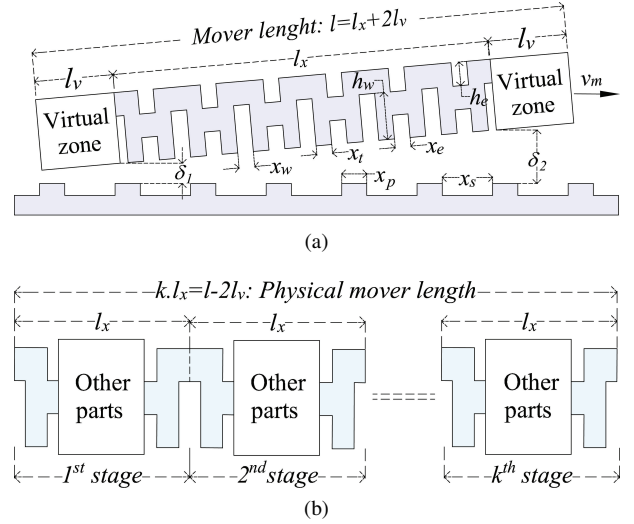


Fig. 2. Resolver dimensions and illustration of the asymmetric air-gap fault: (a) dimensions for a single stage case (b) a  $k$ -stage resolver

TABLE I  
TURNS MAP FOR A SINGLE STAGE PROPOSED RESOLVER

|                         |        | Excitation: $f$ | Signal: $A$         | Signal: $B$   |
|-------------------------|--------|-----------------|---------------------|---------------|
| 1 <sup>st</sup> stage   | 1      | $N_f \odot$     | $\sqrt{3}N_s \odot$ | 0             |
|                         | 2      | $N_f \otimes$   | 0                   | $N_s \odot$   |
|                         | 3      | $N_f \odot$     | 0                   | $N_s \otimes$ |
|                         | 4      | $N_f \otimes$   | $\sqrt{3}N_s \odot$ | 0             |
|                         | 5      | $N_f \odot$     | 0                   | $N_s \odot$   |
|                         | 6      | $N_f \otimes$   | 0                   | $N_s \otimes$ |
| ...                     | ...    | ...             | ...                 | ...           |
| $k$ <sup>st</sup> stage | $6k-5$ | $N_f \odot$     | $\sqrt{3}N_s \odot$ | 0             |
|                         | $6k-4$ | $N_f \otimes$   | 0                   | $N_s \odot$   |
|                         | $6k-3$ | $N_f \odot$     | 0                   | $N_s \otimes$ |
|                         | $6k-2$ | $N_f \otimes$   | $\sqrt{3}N_s \odot$ | 0             |
|                         | $6k-1$ | $N_f \odot$     | 0                   | $N_s \odot$   |
|                         | $6k$   | $N_f \otimes$   | 0                   | $N_s \otimes$ |

has a lower position error than the VR type that is another advantage of the proposed resolver. Since the end-effect is an essential factor considered in linear structures, two virtual air zones are applied to model this effect shown in Fig. 2a [6], [23]. Applying a high-frequency voltage source with frequency  $f_e$  to the excitation winding, as written in Eq. (1), the induced voltages in the open-circuit signal windings ( $A$  and  $B$ ) are used for the position estimation. Considering  $V_{\text{sine}}(t)$  and  $V_{\text{cosine}}(t)$  as the envelope functions of  $V_A(t)$  and  $V_B(t)$ , respectively, the calculated position can be obtained according to Eq. (2) (see Fig. 2 in [6]), where  $x_{\text{cal}}(t)$ ,  $x_{\text{act}}(t)$ , and  $x_{\text{err}}(t)$  are the calculated position, actual position and position error, respectively.

$$v_f(t) = V_{\text{max}} \sin(2\pi f_e t) \quad (1)$$

$$\begin{cases} x_{\text{cal}}(t) = \frac{x_p + x_s}{2\pi} \times \tan^{-1} \left( \frac{V_{\text{sine}}(t)}{V_{\text{cosine}}(t)} \right) \\ x_{\text{err}}(t) = x_{\text{act}}(t) - x_{\text{cal}}(t) \end{cases} \quad (2)$$

The length  $\tau_s = x_p + x_s$  in Eq. (2) is the stator pole pitch. It will be shown that a single-cycle of the signal voltages will be produced per pitch. Hence,  $l_x/\tau_s$  cycles will be produced per mover length ( $l$ ).

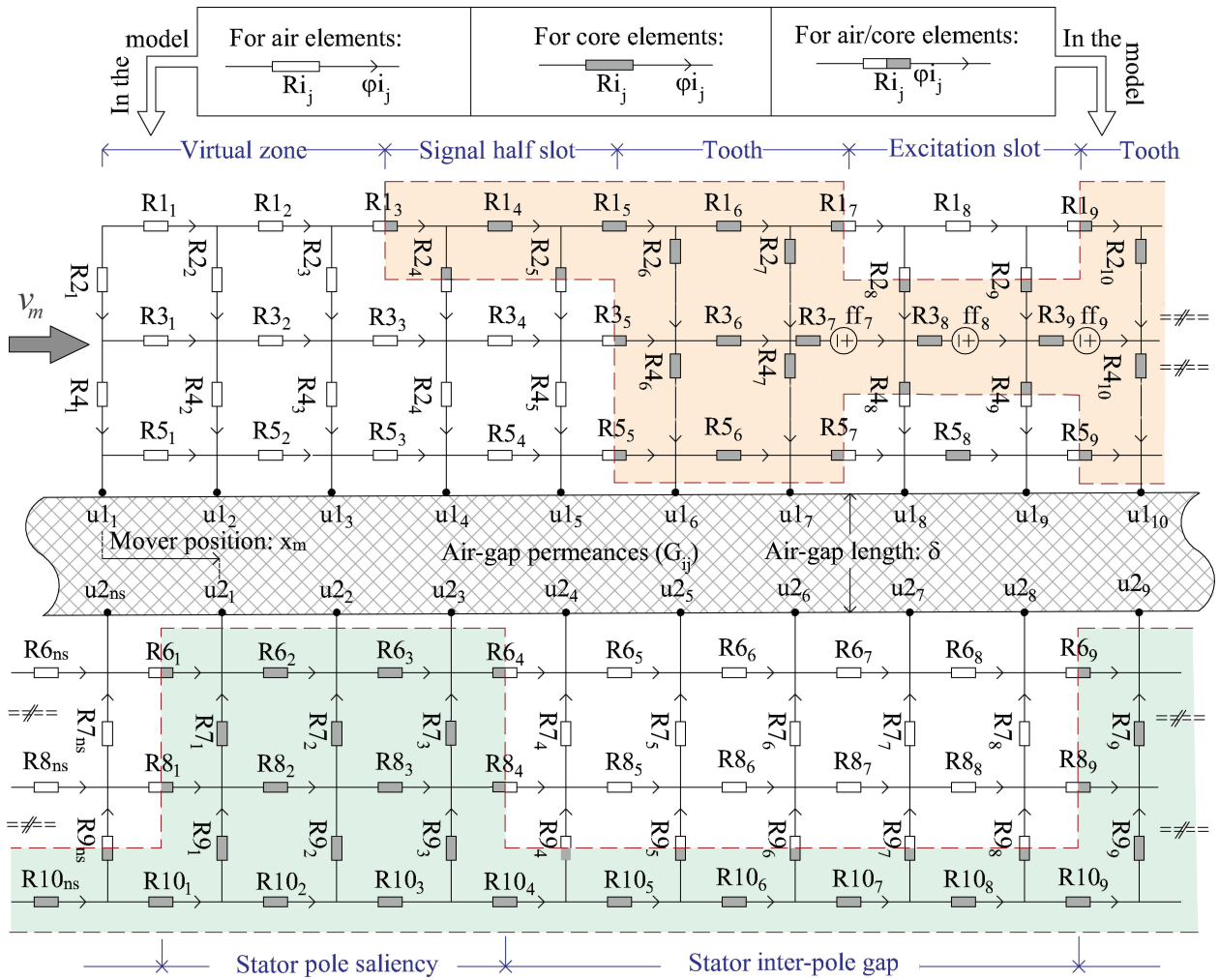


Fig. 3. Considered MEC model for the proposed resolver [23] with a sample accuracy ( $n_v = 3$ ,  $n_t = n_f = 2$ ,  $n_w = 4$ ,  $n_p = 3$ ,  $n_g = 5$ )

### III. CONSIDERED MEC MODEL

A 10-zone MEC model, as shown in Fig. 3, is considered for modeling, where an arbitrary number of flux tubes can be considered for each zone. Hence, a flexible MEC with adjustable accuracy can be obtained for the modeling aim. In order to accurately adjust the model performance, the number of the flux tubes can be selected arbitrarily, as written in Table II. Considering the selected numbers, the total numbers of the flux tubes in various zones are written in Table III, where a circular form with a bigger length ( $l_s = k_s \cdot l$ , and  $k_s \geq 2$ ) is considered for the stator structure [23].

#### A. Main Variables

Noticing Fig. 3, the fluxes of some zones are dependent on the other ones as written in Eq. (3). Hence the fluxes in Eq. (3) are omitted in the equations. The  $\mathbf{Am}$  and  $\mathbf{As}$  matrices are written as Eqs. (4) and (5). Moreover, the system variables are illustrated in Table IV. Considering  $\mathbf{Mf}$ , and  $\mathbf{Ms}$  as the turn function of the windings [6], [24], Eqs. (6) and (7) can be written for the flux linkages

and induced voltages, respectively, where  $R_f$  denotes the resistance of the excitation winding.

$$\begin{cases} \Phi 2 = \mathbf{Am}\Phi 1 \\ \Phi 4 = \mathbf{Am}\Phi 1 + \mathbf{Am}\Phi 3 \\ \Phi 9 = \mathbf{As}\Phi 10 \\ \Phi 7 = \mathbf{As}\Phi 10 + \mathbf{As}\Phi 8 \end{cases} \quad (3)$$

$$\mathbf{Am}_{n_m \times (n_m - 1)} = \begin{bmatrix} -1 & 0 & \dots & \dots & \dots & 0 \\ 1 & -1 & 0 & \dots & \dots & 0 \\ 0 & 1 & -1 & 0 & \dots & 0 \\ \vdots & \ddots & \ddots & \ddots & \ddots & \vdots \\ 0 & \dots & \dots & \dots & 1 & -1 \\ 0 & \dots & \dots & \dots & 0 & 1 \end{bmatrix} \quad (4)$$

$$\mathbf{As}_{n_s \times n_s} = \begin{bmatrix} 1 & -1 & 0 & \dots & \dots & 0 \\ 0 & 1 & -1 & 0 & \dots & 0 \\ \vdots & \ddots & \ddots & \ddots & \ddots & \vdots \\ 0 & \dots & \dots & \dots & 1 & -1 \\ -1 & \dots & \dots & \dots & 0 & 1 \end{bmatrix} \quad (5)$$

TABLE II  
SELECTIVE PARAMETERS FOR ACCURACY ADJUSTING

| Parameter | Definition   |
|-----------|--|
| $n_v$     | Number of the flux tubes per virtual zone          |
| $n_t$     | Number of the flux tubes per mover tooth           |
| $n_w$     | Number of the flux tubes per mover signal slot     |
| $n_f$     | Number of the flux tubes per mover field slot      |
| $n_p$     | Number of the flux tubes per stator pole           |
| $n_g$     | Number of the flux tubes per stator inter-pole gap |

TABLE III  
NUMBER OF FLUX TUBES IN THE PROPOSED MEC ZONES IN FIG. 3

| Zone number    | Total number of flux tubes                    |
|----------------|---|
| 1, 3, 5        | $2n_v + 6k.(n_f + n_w + 2.n_t) - 1 = n_m - 1$ |
| 2, 4           | $2n_v + 6k.(n_f + n_w + 2.n_t) = n_m$         |
| 6, 7, 8, 9, 10 | $l_s/(x_p + x_g).(n_p + n_g) = n_s$           |

TABLE IV  
NUMBER OF VARIABLES IN WHOLE SYSTEM

| Vectors and number of variables                     |           |                             |
|---|-----------|-----------------------------|
| Variables vectors                                   | Number    | Definition                  |
| $\Phi 1 = [\varphi 1_1 \dots \varphi 1_{n_m-1}]^T$  | $n_m - 1$ | Flux of 1st zone            |
| $\Phi 3 = [\varphi 3_1 \dots \varphi 3_{n_m-1}]^T$  | $n_m - 1$ | Flux of 3rd zone            |
| $\Phi 5 = [\varphi 5_1 \dots \varphi 5_{n_m-1}]^T$  | $n_m - 1$ | Flux of 5th zone            |
| $\Phi 6 = [\varphi 6_1 \dots \varphi 6_{n_s}]^T$    | $n_s$     | Flux of 6th zone            |
| $\Phi 8 = [\varphi 8_1 \dots \varphi 8_{n_s}]^T$    | $n_s$     | Flux of 8th zone            |
| $\Phi 10 = [\varphi 10_1 \dots \varphi 10_{n_s}]^T$ | $n_s$     | Flux of 10th zone           |
| $i_f$   | 1         | Excitation winding current  |
| $U1 = [u1_1 \dots u1_{n_m}]^T$                      | $n_m$     | Nodes potentials of air-gap |
| $U2 = [u2_1 \dots u2_{n_m}]^T$                      | $n_s$     | Nodes potentials of air-gap |
| Total number of variables: $n_{var} = 4n_m + 4n_s$  |           |                             |

$$\begin{cases} \lambda_f = \mathbf{Mf}\Phi 3 \\ \Lambda_{sig} = [\lambda_A \quad \lambda_B]^T = \mathbf{MsAm}\Phi 1 + 0.5\mathbf{MsAm}\Phi 3 \end{cases} \quad (6)$$

$$v_f = \frac{d\lambda_f}{dt} + R_f.i_f, \quad v_A = \frac{d\lambda_A}{dt}, \quad v_B = \frac{d\lambda_B}{dt} \quad (7)$$

Considering  $\Delta t$  as the time-step, applying the trapezoidal method to the Eq. (7), the converted equation is written as Eq. (8).

$$\begin{aligned} \mathbf{Mf}\Phi 3(t) + \frac{\Delta t}{2} R_f.i_f(t) = \\ \frac{\Delta t}{2} \left( v_f(t) + v_f(t - \Delta t) \right) + \mathbf{Mf}\Phi 3(t - \Delta t) \triangleq C \end{aligned} \quad (8)$$

### B. Air-gap Permeances

Air-gap permeances are the most important part of a MEC-based model that calculates the air-gap flux. Considering  $m$  as the asymmetry index in Eq. (16), the permeance between the  $i^{\text{th}}$  mover and  $j^{\text{th}}$  stator flux tubes function ( $G'$ ) is computed by Eq. (12) based on Eqs. (9)-(11).

$$\vartheta(\theta_{act}) = \log \left( \frac{\cosh(\pi \frac{\theta_{act} - \gamma_t}{2\beta}) \cosh(\pi \frac{\theta_{act} + \gamma_t}{2\beta})}{\cosh(\pi \frac{\theta_{act}}{2\beta}) \cosh(\pi \frac{\theta_{act}}{2\beta})} \right) - \frac{\gamma_t^2}{2\beta} \quad (9)$$

$$G(\theta_{act}) = \frac{\vartheta(\theta_{act}) - \vartheta(\pi)}{\vartheta(0) - \vartheta(\pi)} \quad (10)$$

$$Gp(\theta_{act}) = \sum_{k=-1}^1 G(\theta_{act} - 2k\pi) \quad (11)$$

$$G'(\theta_{act}, i, j) = Gp \left( \theta_{act} - (i-1)\gamma_m + (j-1)\gamma_s \right) \quad (12)$$

In the Eqs. (9)-(12):

$$\begin{cases} \gamma_m = \frac{2\pi \times (l/l_s)}{n_m}, \gamma_s = \frac{2\pi}{n_s}, \gamma_t = \max(\gamma_s, \gamma_m) \\ \beta = \log \left( \frac{l_s + 2\pi\delta}{l_s} \right), \delta = \frac{1}{2}(\delta_1 + \delta_2) \\ \theta_{act} = \frac{2\pi}{l_s} \times x_{act} \end{cases} \quad (13)$$

$G_m$  is defined as the bellow function, where the  $g(\theta_{act}, i, m)$  is the air-gap function.

$$G_m(\theta_{act}, i, m) = \mu_0 \times l \times \frac{\min(l_s/n_s, l/n_m)}{g(\theta_{act}, i, m)} \quad (14)$$

The permeance between the given  $i$  and  $j$  nodes ( $G_{ij}$ ) can be computed by Eq. (15), where the gap function is written in Eq. (16).

$$G_{ij}(\theta_{act}) \triangleq G_m(\theta_{act}, i, m)G'(\theta_{act}, i, j) \quad (15)$$

$$\begin{cases} g(\theta_{act}, i, m) = \delta_1 + \gamma_m(i-1)m - \frac{l_v}{l_m}(\delta_2 - \delta_1) \\ m = (\delta_2 - \delta_1) \frac{l_s/(2\pi) + \delta}{l_x} \end{cases} \quad (16)$$

Considering  $v_m(t)$  as the mover speed, the actual rotor position ( $\theta_{act}$ ) is computed as Eq. (17)

$$\begin{cases} x_{act}(t) = v_m(t).t + x_{act}(0) \\ \theta_{act}(t) = \frac{2\pi}{l_s} v_m(t).t + \frac{2\pi}{l_s} x_{act}(0), \quad \frac{2\pi}{l_s} x_{act}(0) = \theta_{act}(0) \end{cases} \quad (17)$$

### C. Equation Solving

Considering the defined equations and presented details in [23], the whole equation system can be defined by Eq. (18). These equations should be solved for each time-step ( $\Delta t$ ). Although the solving procedure is illustrated in algorithm 1, the equation details can be found in [23], where the matrices computation and reluctance of the flux tubes for a saturable core are illustrated.

## IV. EVALUATION BY SIMULATION RESULTS

In view of performance evaluation, simulation results are evaluated under the following considerations:

⊛-Two individual resolvers (single and double stages) are evaluated under the healthy case. The resolver properties are tabulated in Table V.

⊛-Influence of the asymmetry air-gap with  $\delta_1 = 0.25$  mm,  $\delta_2 = 0.75$  mm is analyzed.

⊛-Since the Resolver to Digital (R/D) converter [3] is not investigated in this paper, Hilbert's transformation and a written m-file in Matlab are used to obtain the envelope functions of the induced voltage of the signal windings [5], [6], [20]. Although the R/D converter has a very small delay in practice due to sampling time, that is usually neglected thanks to high-speed processors.

⊛-The mover speed is considered as  $v_m = 1$  m/s.

⊛-Excitation voltage with  $V_{max} = 12$  V amplitude and  $f_e = 5$  kHz is considered for all cases.

$$\mathbf{A} \left( \mathbf{X}(t) \right) \mathbf{X}(t) = \mathbf{B}(t, t - \Delta t) \quad (18a)$$

$$\begin{bmatrix} 0 & \mathbf{Mf} & 0 & 0 & 0 & 0 & \Delta t/2R_f & 0 & 0 \\ \mathbf{M1} & -\mathbf{R3} & 0 & 0 & 0 & 0 & \mathbf{Wf} & 0 & 0 \\ \mathbf{M2} & \mathbf{M3} & -\mathbf{R5} & 0 & 0 & 0 & -\mathbf{Wf} & 0 & 0 \\ 0 & 0 & \mathbf{R5} & 0 & 0 & 0 & 0 & -\mathbf{Au} & 0 \\ 0 & 0 & 0 & \mathbf{R6} & 0 & 0 & 0 & 0 & -\mathbf{As} \\ 0 & 0 & 0 & -\mathbf{R6} & \mathbf{M4} & \mathbf{M5} & 0 & 0 & 0 \\ 0 & 0 & 0 & 0 & -\mathbf{R8} & \mathbf{M6} & 0 & 0 & 0 \\ -\mathbf{Am} & -\mathbf{Am} & -\mathbf{Am} & 0 & 0 & 0 & 0 & \mathbf{App} & \mathbf{Aps} \\ 0 & 0 & 0 & -\mathbf{As} & -\mathbf{As} & -\mathbf{As} & 0 & \mathbf{Asp} & \mathbf{Ass} \end{bmatrix} \cdot \begin{bmatrix} \Phi 1 \\ \Phi 3 \\ \Phi 5 \\ \Phi 6 \\ \Phi 8 \\ \Phi 10 \\ i_f \\ \mathbf{U1} \\ \mathbf{U2} \end{bmatrix} = \begin{bmatrix} C \\ 0 \\ 0 \\ 0 \\ 0 \\ 0 \\ 0 \\ 0 \\ 0 \end{bmatrix} \quad \text{where,} \quad \begin{cases} \mathbf{M1} = \mathbf{R1} + \mathbf{R2Am} \\ \mathbf{M2} = \mathbf{R4Am} \\ \mathbf{M3} = \mathbf{R3} + \mathbf{R4Am} \\ \mathbf{M4} = \mathbf{R7As} \\ \mathbf{M5} = \mathbf{R8} + \mathbf{R7As} \\ \mathbf{M6} = \mathbf{R10} + \mathbf{R9As} \\ \mathbf{Wf} = \mathbf{Mf}^T \end{cases} \quad (18b)$$

⊗-The position error at  $x_{act}(k \times \tau_s)$  for  $k = 0, 1, 2, \dots$  is considered as the absolute position error (APE), where  $\tau_s = x_p + x_s$ .

G-In the proposed resolver, the zero position reference is obtained by aligning p1 and p2 points as shown in Fig. 4. Hence the initial position in the used MEC model should be considered as Eq. (19).

⊗-Simulations are performed for  $0 \leq x_{act} \leq 4l_s$ , where the results are shown in  $l_s \leq x_{act} \leq 3l_s$  to avoid the dynamic transients of the excitation current and Hilbert's transformation. Considering  $x_{act}(0)$  in Eq. (19), the results are scaled by  $0 \leq x_{act} \leq 2l_s$ .

$$\begin{cases} x_{act}(0) = x_1 - x_2 \\ x_1 = l_v - \frac{l}{2n_m} + 5(2x_t + x_w + x_e) \\ x_2 = \frac{11}{2}x_p + 5x_g - \frac{l_s}{2n_s} \end{cases} \quad (19)$$

TABLE V  
PROPERTIES OF THE SIMULATED RESOLVERS

|                                | Parameter  | Symb.         | Value |
|--------------------------------|--|---------------|-------|
| Dimensions (mm)                | Height of the field slot                               | $h_e$         | 6     |
|                                | Height of the signal slot                              | $h_w$         | 12    |
|                                | Height of the stator pole                              | $h_p$         | 2     |
|                                | Height of the stator yoke                              | $h_y$         | 4     |
|                                | Width of the mover tooth                               | $x_t$         | 4     |
|                                | Width of the mover signal slot                         | $x_w$         | 4     |
|                                | Width of the mover field slot                          | $x_e$         | 4     |
|                                | Width of the stator pole                               | $x_p$         | 6.4   |
|                                | Width of the stator inter-pole gap                     | $x_s$         | 12.8  |
|                                | Machine width in z axis                                | $l_z$         | 10    |
|                                | Physical length of the mover                           | $l$           | 96    |
|                                | Air-gap length in healthy case                         | $\delta$      | 0.5   |
| Electrical                     | Turns per each field coil                              | $N_f$         | 20    |
|                                | Turns per each coil of winding A                       | $\sqrt{3}N_s$ | 35    |
|                                | Turns per each coil of winding B                       | $N_s$         | 20    |
|                                | Field winding resistance for single stage ( $\Omega$ ) | $R_f$         | 1     |
|                                | Field winding resistance for double stage ( $\Omega$ ) | $R_f$         | 2     |
| Accuracy                       | Virtual zones length (cm)                              | $l_v$         | 2     |
|                                | Length of circular secondary for single-stage(cm)      | $l_s$         | 28.8  |
|                                | Length of circular secondary for double-stage(cm)      | $l_s$         | 48    |
|                                | Number of flux tubes per $l_v$                         | $n_v$         | 10    |
|                                | Number of flux tubes per $x_t$                         | $n_t$         | 2     |
|                                | Number of flux tubes per $x_e$                         | $n_f$         | 2     |
|                                | Number of flux tubes per $x_w$                         | $n_w$         | 2     |
|                                | Number of flux tubes per $x_g$                         | $n_g$         | 4     |
| Number of flux tubes per $x_p$ | $n_p$  | 2             |       |

**Data:** Constant data and constant matrices include:

Resolver properties:  $R_f, k, N_s, N_f, m, x_v, x_t, x_e, x_s, x_p, x_g, \dots$

Desired accuracy:  $n_v, n_t, n_w, n_p, n_g$

Flux tubes length and area:  $Ai_j, li_j^g, li_j^c$  [6], [23]

Compute:  $\mathbf{Ms}, \mathbf{Mf}, \mathbf{As}, \mathbf{Am}, \mathbf{Au}$  [23]

**Result:** Solving nonlinear equations (Eq. (18b))

**Initialization:**  $t = 0, \Delta t$  and  $T_{max}$ : as desired,  $\mathbf{X}(t = 0) = \mathbf{0}$

Initial mover position ( $\theta_{act}(t = 0)$ ) by Eqs. (13) and (19)

Compute:  $G_{ij}(\theta_{act})$  by Eq. (15);

Acceptable error:  $er = 1 \times 10^{-8}$

Maximum iteration number:  $k_{max}$

Mover speed:  $v_m(t)$  and excitation voltage:  $v_f(t)$

**while**  $t \leq T_{max}$  **do**

initialization;

Iteration index:  $k = 1$

$\mathbf{X}(t)^{(0)} = \mathbf{X}(t)$

Compute:  $\mathbf{Ass}(\theta_{act}(t)), \mathbf{App}(\theta_{act}(t)), \mathbf{Aps}(\theta_{act}(t))$

**while**  $k \leq k_{max}$  **do**

Compute:  $\mathbf{R1}(\mathbf{X}(t)^{(k-1)}) \dots \mathbf{R10}(\mathbf{X}(t)^{(k-1)})$ ;

Compute:  $\mathbf{A}(\mathbf{X}(t)^{(k-1)}), \mathbf{B}$ ;

Compute: Jacobian matrix,  $\mathbf{J}(\mathbf{X}(t)^{(k-1)})$ ;

Compute:  $\Delta \mathbf{Y} = \mathbf{B} - \mathbf{A}(\mathbf{X}(t)^{(k-1)})\mathbf{X}(t)^{(k-1)}$

Compute:  $\Delta \mathbf{X}(t)^{(k)} = \mathbf{J}(\mathbf{X}(t)^{(k-1)})^{-1} \Delta \mathbf{Y}$

**if** Max.  $\Delta \mathbf{X}(t)^{(k)} \leq er$  **then**

$\mathbf{X}(t)^{(k)} = \mathbf{X}(t)^{(k-1)}$

Compute:  $V_A(t)$  and  $V_B(t)$  by Eqs. (6) and (7)

Compute: Envelopes and  $x_{cal}(t), x_{err}(t)$  by Eq. (2)

Compute: Mover position  $x_{act}(t), \theta_{act}(t)$  by Eq. (17)

$t = t + \Delta t$

**else**

$k = k + 1$

$\mathbf{X}(t)^{(k)} = \mathbf{X}(t)^{(k-1)} + \Delta \mathbf{X}(t)^{(k)}$

**end**

**end**  
 $\mathbf{X}(t) = \mathbf{X}(t)^{(k)}$

**end**

**Algorithm 1:** Procedure of the equations solving

### A. Performance Analysis of the Single-Stage Resolvers

The single-stage resolver performance is analyzed in this part, where maximum and absolute position errors (MPE and APE) are evaluated. Obtained results for healthy and faulty resolvers are shown in Figs. 5 and 6, where induced voltages, envelope functions (by Hilbert's transformation and a written m-file), and position errors are included in the results.

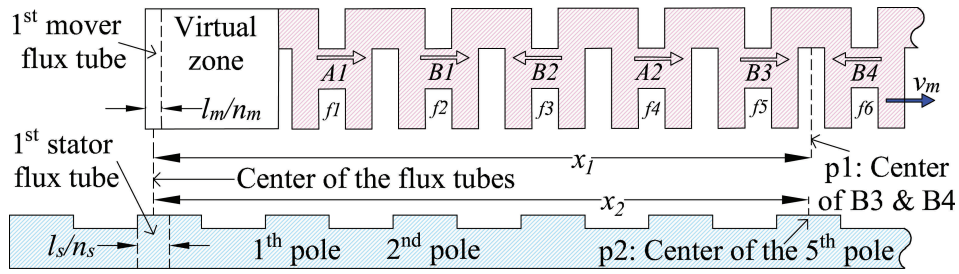
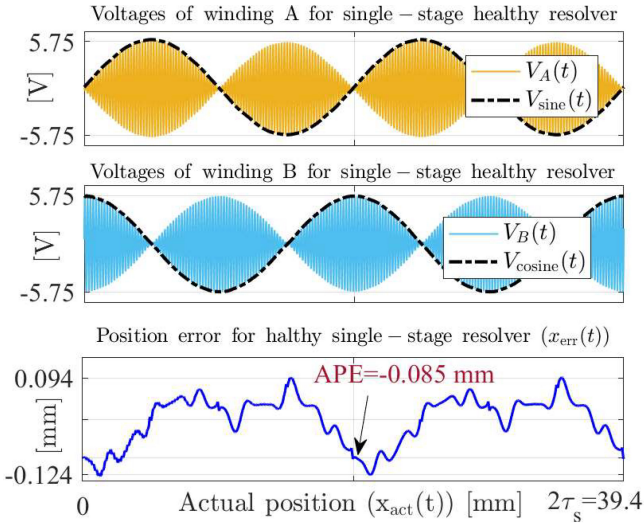
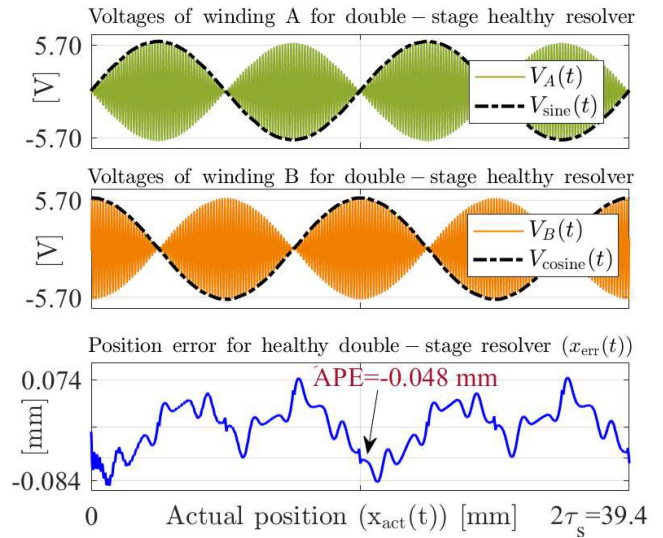
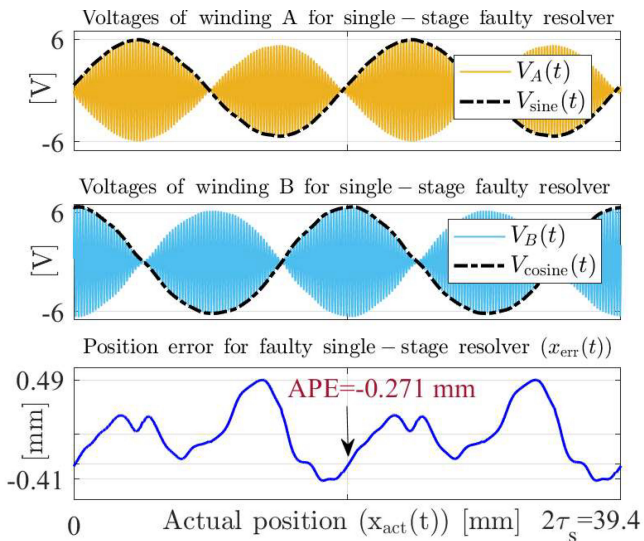
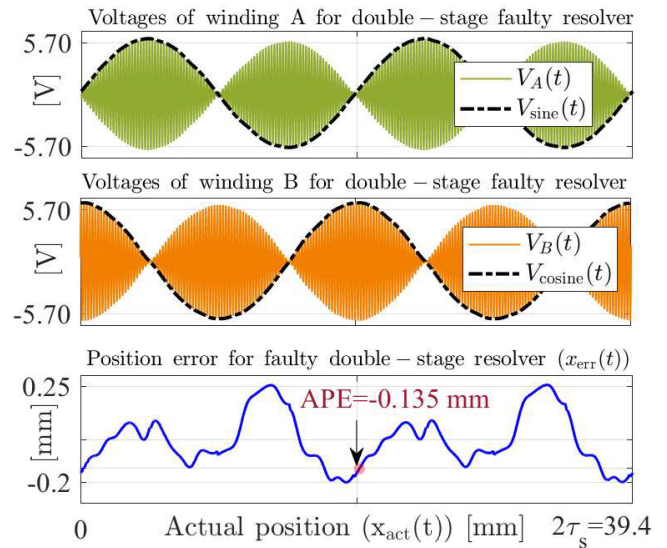


Fig. 4. Illustration of the mover position and its initial value in the MEC model


 Fig. 5. Induced voltages, envelopes, and position error for the healthy single-stage resolver under  $v_m(t) = 1$  m/s

 Fig. 7. Induced voltages, envelopes, and position error for the healthy double-stage resolver under  $v_m(t) = 1$  m/s

 Fig. 6. Induced voltages, envelopes, and position error for the faulty single-stage resolver under  $v_m(t) = 1$  m/s

 Fig. 8. Induced voltages, envelopes, and position error for the faulty double-stage resolver under  $v_m(t) = 1$  m/s

### B. Performance Analysis of the Double-Stage Resolvers

The MPE and APE of the double-stage resolver are obtained, and the results are shown in Figs. 7 and 8.

Moreover, the non-equal magnetic circuit of the signal windings is less investigatable than the single-stage one. Hence performance enactment is obtained. Results of the position errors are tabulated in Table VI.

TABLE VI  
OBTAINED MPE AND APE FOR THE ANALYZED RESOLVERS

| Type   | Healthy resolver |          | Faulty resolver |          |
|--------|------------------|----------|-----------------|----------|
|        | MPE (mm)         | APE (mm) | MPE (mm)        | APE (mm) |
| Single | 0.124            | -0.085   | 0.490           | -0.271   |
| Double | 0.084            | -0.048   | 0.250           | -0.135   |

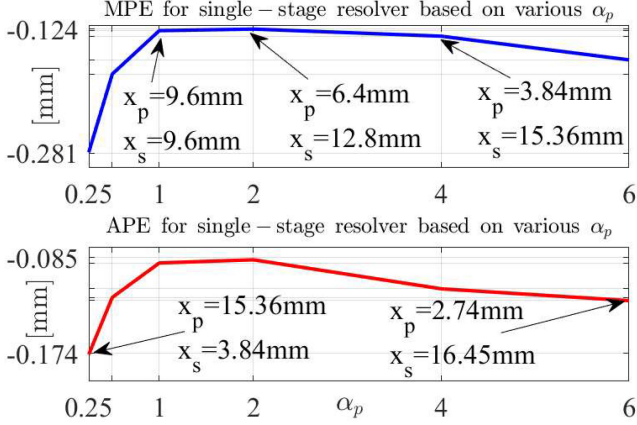


Fig. 9. Obtained MPE and APE for single-stage healthy resolver

As is clear, the position error in the double-stage type is reduced thanks to the end-effect reduction. Additionally, noticing the results, one cycle of the induced voltages and their envelopes are produced per pitch ( $\tau_s = x_p + x_s$ ). Hence there are  $5k$  cycles of the envelopes per the mover length.

### C. Influence of the Stator Pole Width

In order to analysis of the stator pole width, the single-stage resolver with parameters listed in Table V is considered for analysis. The resolver performance under constant pole pitch ( $\tau_s = x_p + x_s$ ) is evaluated under various  $\alpha_p$  as written in Eq. (20).

$$x_s = \alpha_p \cdot x_p \Rightarrow x_p = \frac{\tau_s}{1 + \alpha_p} \quad (20)$$

Results of the MPE and APE for the considered resolver under healthy and defined faulty cases are shown in Fig. 9 for various  $\alpha_p$ . As is clear from the figure, the best position error is obtained by  $\alpha_p = 2$ , where 0.124 mm and 0.085 mm are obtained for the MPE and APE, respectively.

### D. Comparison with Variable Reluctance Linear Resolver

Performance of the presented single-stage resolver can be compared with the analyzed Variable Reluctance Linear Resolver (VR-L-Resolver) in [6]. In [6] a VR-L-Resolver with both overlapping and non-overlapping windings is studied. The same mover and air-gap lengths ( $l = 96$  mm,  $\delta = 0.5$  mm) as well as the same analyses compared to this work were performed for healthy and faulty cases. Both types have the same structure in which the windings are located on the mover. Therefore comparison can be performed between them. The result of the comparison is presented in Table VII. As is clear, the presented resolver in the healthy case has better accuracy compared to the healthy VR-L type with both overlapping and non-overlapping windings.

TABLE VII  
COMPARISON BETWEEN THE PROPOSED AND VR-L RESOLVERS IN HEALTHY AND FAULTY CASES

|     | Healthy case ( $\delta_1 = \delta_2 = 0.5$ mm)          |                   |                   |
|-----|---|-------------------|-------------------|
|     | Proposed  | VR-L-Resolver     |                   |
|     |   | Overlapping       | Non-Overlapping   |
| MPE | 124 $\mu\text{m}$                                       | 770 $\mu\text{m}$ | 333 $\mu\text{m}$ |
| APE | 85 $\mu\text{m}$  | 12 $\mu\text{m}$  | 12 $\mu\text{m}$  |
|     | Faulty case ( $\delta_1 = 0.25$ , $\delta_2 = 0.75$ mm) |                   |                   |
|     | Proposed  | VR-L-Resolver     |                   |
|     |   | Overlapping       | Non-Overlapping   |
| MPE | 490 $\mu\text{m}$                                       | 900 $\mu\text{m}$ | 2.62 mm           |
| APE | 271 $\mu\text{m}$                                       | 180 $\mu\text{m}$ | 1.98 mm           |

Moreover, less sensitivity to the asymmetry air-gap fault is obtained for the presented resolver. Hence, the introduced novel resolver is a better choice compared to the VR type.

### E. Some Important Notes for Accuracy Improvement

Noticing the performed research, there are some valuable notes that should be considered for the proposed resolver design. All of the following issues must be respected to obtain an optimized design resolver with error sources weakening.

1- Since the number of turns in winding A in  $\sqrt{3}$  times greater than the number of turns in winding B (see Table I), smaller APE and MPE can be obtained by smaller defined  $k_w$  in the Eq. (21).

$$k_w = \left| \frac{\sqrt{3}N_s - \text{Round}(\sqrt{3}N_s)}{\sqrt{3}N_s} \right| \quad (21)$$

Clearly,  $k_w = 0$  denotes the integer number of the turns in the winding A that allows having minimum APE and MPE. Therefore, considering the slots space of the mover, the  $N_s$  value should be considered based on the obtaining of the minimum  $k_w$  values. Using  $N_s = 20$  for the designed resolver,  $k_w = 0.0103$  is obtained as the mentioned value.

2- Noticing Eq. (20) and the defined  $\alpha_p$  parameters as well as performed results in Fig. 9, the minimum APE and MPE are obtained by a certain  $\alpha_p$  value.

3- The nd-effect is one of the most important phenomena in the linear machines and actuators [23] that caused error production in the linear resolvers [6], [9]. This phenomenon can be reduced by the mover length increasing. Hence for a  $k$ -stage proposed resolver, the APE and MPE reduction can be obtained by a higher  $k$  value.

4- The excitation frequency is an important factor in the resolvers' accuracy that should be high enough based on the mover speed, where the number of high-frequency cycles per low-frequency cycle should be high to obtain an accurate envelope wave [5]. However, the core material should be chosen based on the excitation frequency due to the eddy current effect phenomenon.

5- The produced noise from electromagnetic sources is

the most important component of noise. Although this can affect the induced voltages of the windings, the signal-to-noise ratio is high thanks to high-amplitude produced main voltages. Noticing the obtained results in Figs. 5-8, the induced voltages with 6 V amplitude are obtained. Hence the number of turns for signal windings and current of the excitation winding must be chosen wisely to obtain high-amplitude signal voltages. The noise effect can be neglected in this case.

## V. EXPERIMENTAL RESULTS

The single-stage resolver with tabulated parameters in Table V is manufactured for experimental validation. The mover and stator cores are made by silicon-steel powder (Fe-6.5wt%Si) that allows having low eddy current without the core lamination. The manufactured resolver and the used setup are shown in Figs. 10 and 11. Moreover, a belt-connected DC motor is used for the mover movement. In addition, the air-gap asymmetry for the faulted resolver test is produced by the mover displacement on the mover case. The induced voltages in the stationary case at  $x_{act}(0) = 0$  are shown in Fig. 12. In the healthy and defined faulty cases, position errors are computed by the amplitudes extracted from signal windings. The results of the healthy and faulty resolvers are shown in Figs. 13 and 14, respectively. Noticing the results, there is an excellent agreement between the simulation and experimental results in both healthy and faulty cases. Hence, the effectiveness of the proposed novel resolver is proved.

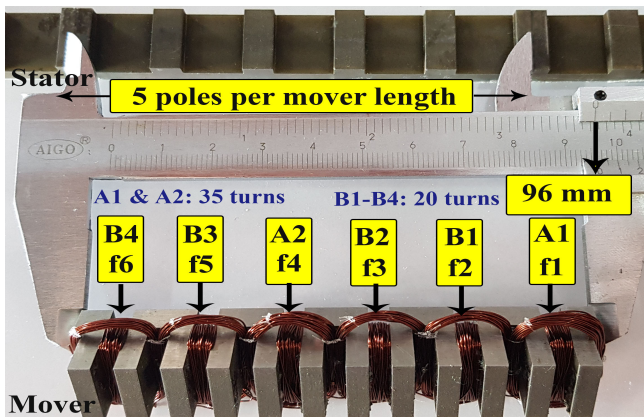


Fig. 10. Mover, stator, and windings of the manufactured resolver

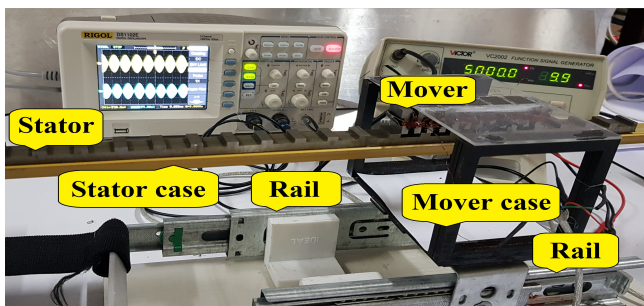


Fig. 11. The used setup for experimental validation

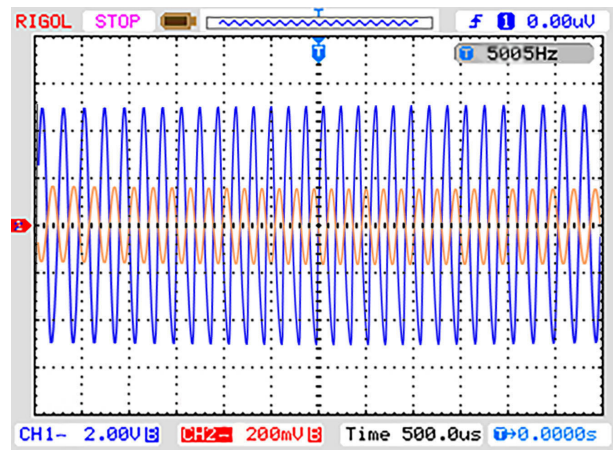


Fig. 12. Experimental  $V_A(t)$  and  $V_B(t)$  under  $v_m = 0$  and  $x_{act}(t) = 0$

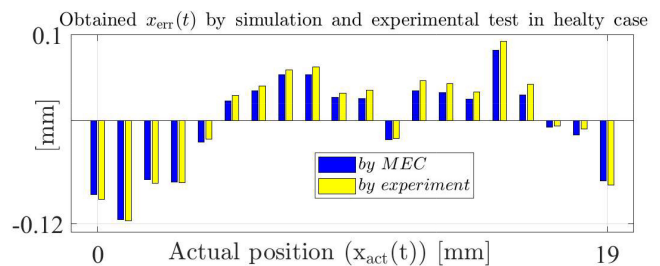


Fig. 13. Obtained position error in 20 individual mover positions by simulation and experimental test for healthy resolver

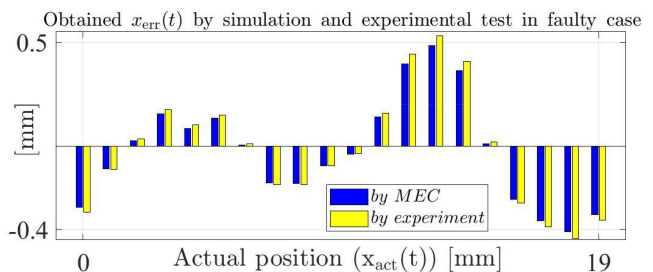


Fig. 14. Obtained position error in 20 individual mover positions by simulation and experimental test for faulty resolver

## VI. CONCLUSION

A novel linear resolver is proposed in this paper, where the excitation and signals windings are located on the mover. The simple structure and acceptable position error are the advantages of the proposed resolver compared to the Variable Reluctance type. Although the single and double stages resolvers are analyzed, the  $k$ -stage structure ( $k = 1, 2, \dots$ ) is possible, where the position estimation is more accurate for a higher value of  $k$ . A flexible Magnetic Equivalent Circuit is used for modelling thanks to its capability, where various cases are modeled for performance evaluation. Noticing the used MEC flexibility and performed iterative simulations, the mentioned method is a better choice for these simulations types than the FEM that caused more flexibility and shorter processing time. Hence it is suggested for further research. The proposed linear resolver and performance analysis in healthy and faulty cases are the paper novelties, where its effectiveness is validated by experimental results.



## REFERENCES

- [1] Z. Nasiri-Gheidari and F. Tootoonchian, "Axial flux resolver design techniques for minimizing position error due to static eccentricities," *IEEE Sensors Journal*, vol. 15, no. 7, pp. 4027–4034, 2015.
- [2] H. Zumbahlen, "Phase response in active filters; part 2, the low-pass and high-pass response," *Analog Devices Report*, 2009.
- [3] W. Lee, J.-J. Moon, W.-S. Im, J.-H. Park, and J.-M. Kim, "Classification and compensation of dc offset error and scale error in resolver signals," *Journal of Power Electronics*, vol. 16, no. 3, pp. 1190–1199, 2016.
- [4] Z. Nasiri-Gheidari, F. Tootoonchian, and F. Zare, "Design oriented technique for mitigating position error due to shaft run-out in sinusoidal-rotor variable reluctance resolvers," *IET Electric Power Applications*, vol. 11, no. 1, pp. 132–141, 2017.
- [5] P. Naderi, R. Ghandehari, and M. Heidary, "A comprehensive analysis on the healthy and faulty two types vr-resolvers with eccentricity and inter-turn faults," *IEEE Transactions on Energy Conversion*, vol. 36, DOI 10.1109/TEC.2021.3079725, no. 4, pp. 3502–3511, 2021.
- [6] P. Naderi, A. Ramezannezhad, and L. Vandeveld, "Performance analysis of variable reluctance linear resolver by parametric magnetic equivalent circuit in healthy and faulty cases," *IEEE Sensors Journal*, vol. 21, no. 18, pp. 19912–19921, 2021.
- [7] X. Ge and Z. Zhu, "A novel design of rotor contour for variable reluctance resolver by injecting auxiliary air-gap permeance harmonics," *IEEE Transactions on Energy Conversion*, vol. 31, no. 1, pp. 345–353, 2015.
- [8] L. Xiao, Z. Li, and C. Bi, "An optimization approach to variable reluctance resolver," *IEEE Transactions on Magnetics*, vol. 56, no. 2, 2020.
- [9] A. Daniar, Z. Nasiri-Gheidari, and F. Tootoonchian, "Performance analysis of linear variable reluctance resolvers based on an improved winding function approach," *IEEE Transactions on Energy Conversion*, vol. 33, no. 3, pp. 1422–1430, 2018.
- [10] A. Daniar, Z. Nasiri-Gheidari, and F. Tootoonchian, "Position error calculation of linear resolver under mechanical fault conditions," *IET Science, Measurement & Technology*, vol. 11, no. 7, pp. 948–954, 2017.
- [11] Z. Nasiri-Gheidari, "Design, performance analysis, and prototyping of linear resolvers," *IEEE Transactions on Energy Conversion*, vol. 32, no. 4, pp. 1376–1385, 2017.
- [12] H. Saneie, Z. Nasiri-Gheidari, and F. Tootoonchian, "Analytical model for performance prediction of linear resolver," *IET Electric Power Applications*, vol. 11, no. 8, pp. 1457–1465, 2017.
- [13] A. Paymozd, H. Saneie, Z. Nasiri-Gheidari, and F. Tootoonchian, "Subdomain model for predicting the performance of linear resolver considering end effect and slotting effect," *IEEE Sensors Journal*, vol. 20, no. 24, pp. 14747–14755, 2020.
- [14] M. Bahari, R. Alipour-Sarabi, Z. Nasiri-Gheidari, and F. Tootoonchian, "Proposal of winding function model for geometrical optimization of linear sinusoidal area resolvers," *IEEE Sensors Journal*, vol. 19, no. 14, pp. 5506–5513, 2019.
- [15] A. Paymozd, H. Saneie, A. Daniar, and Z. Nasiri-Gheidari, "Accurate and fast subdomain model for electromagnetic design purpose of wound-field linear resolver," *IEEE Transactions on Instrumentation and Measurement*, vol. 70, DOI 10.1109/TIM.2021.3080400, 2021.
- [16] F. Zare and Z. Nasiri-Gheidari, "Magnetic equivalent circuit model for predicting performance of 2dof wound rotor resolver," *IEEE Sensors Journal*, 2021.
- [17] F. Zare and Z. Nasiri-Gheidari, "Proposal of a 2dof wound-rotor resolver," *IEEE Sensors Journal*, DOI 10.1109/JSEN.2021.3089540, 2021.
- [18] H. Saneie, R. Alipour-Sarabi, Z. Nasiri-Gheidari, and F. Tootoonchian, "Challenges of finite element analysis of resolvers," *IEEE Transactions on Energy Conversion*, vol. 34, DOI 10.1109/TEC.2018.2881465, no. 2, pp. 973–983, 2019.
- [22] F. Tootoonchian, "Proposal of new windings for 5-x variable reluctance resolvers," *IET Science, Measurement & Technology*, vol. 12, no. 5, pp. 651–656, 2018.
- [19] S. Hajmohammadi, H. Saneie, Z. Nasiri-Gheidari, and F. Tootoonchian, "Optimal design and performance analysis of a double-sided multi-turn wound-rotor resolver," *IEEE/ASME Transactions on Mechatronics*, DOI 10.1109/TMECH.2021.3066815, 2021.
- [20] R. Ghandehari, P. Naderi, and L. Vandeveld, "Performance analysis of a new type pm-resolver in healthy and eccentric cases by an improved parametric mec method," *IEEE Transactions on Instrumentation and Measurement*, vol. 70, DOI 10.1109/TIM.2021.3080388, pp. 1–10, 2021.
- [21] M. Bahari and F. Tootoonchian, "Proposal of a fault-tolerance technique for 1-ph open circuit fault in resolvers," *IEEE Sensors Journal*, vol. 21, DOI 10.1109/JSEN.2021.3076173, no. 14, pp. 15987–15992, 2021.
- [23] P. Naderi, M. Heydari, and M. Vahedi, "Performance analysis of ladder secondary linear induction motor with two different secondary types using magnetic equivalent circuit," *ISA Transactions*, vol. 103, pp. 355–365, 2020.
- [24] V. Ostovic, *Dynamics of Saturated Electric Machines*. Springer-Verlag New York, 1989.



**Peyman Naderi** was born in Ahvaz, Iran, in 1975. He received his B.S. degree in Electronic Engineering in 1998 and M.S. degree in Power Engineering from Chamran University, Iran, Ahvaz in 2001. He has a Ph.D. degree in Power Engineering Science from K.N. Toosi University, Tehran, Iran. His interests are electrical machine modeling and fault diagnosis and also power system transient. He is currently associate professor in Shahid Rajaei Teacher Training University of Tehran, Iran.



**Arman Ramezannezhad** was born in Rasht, Iran, in 1982. He received his B.S. degree in electrical engineering from Guilan University, Rasht, Iran, and M.S. degree in power engineering from Tafresh University, Arak, Iran, in 2008 and 2012, respectively. Recently, he is a Ph.D. student at Shahid Rajaei Teacher Training University, Tehran, Iran.



**Lieven Vandeveld** was born in Eeklo, Belgium, in 1968. He received the Ph.D. degree from Ghent University, Ghent, Belgium, in 1997. Currently, he is with the Department of Electromechanical, Systems and Metal Engineering, Ghent University. Since 2004, he has been a Professor of electrical power engineering. His research and teaching activities are in the field of electric power systems, electrical machines, and computational electromagnetics.